



## RESEARCH PAPER

# Early consequences of the phospholamban mutation PLN-R14del<sup>+/-</sup> in a transgenic mouse model

Claudia Maniezzi<sup>1</sup> | Marem Eskandr<sup>1</sup> | Chiara Florindi<sup>1</sup> | Mara Ferrandi<sup>2</sup> | Paolo Barassi<sup>2</sup> | Elena Sacco<sup>1</sup>  | Valentina Pasquale<sup>1</sup> | Angela S. Maione<sup>3</sup> | Giulio Pompilio<sup>3,4</sup> | Vivian Oliveira Nunes Teixeira<sup>5</sup> | Rudolf A. de Boer<sup>6</sup> | Herman H. W. Silljé<sup>5</sup> | Francesco Lodola<sup>1</sup>  | Antonio Zaza<sup>1</sup>

<sup>1</sup>Department of Biotechnology and Bioscience, University of Milano-Bicocca, Milan, Italy

<sup>2</sup>Windtree Therapeutics Inc., Warrington, Pennsylvania, USA

<sup>3</sup>Unit of Vascular Biology and Regenerative Medicine, Centro Cardiologico Monzino IRCCS, Milan, Italy

<sup>4</sup>Department of Biomedical, Surgical and Dentist Sciences, University of Milano, Milan, Italy

<sup>5</sup>Department of Cardiology, University Medical Center Groningen, University of Groningen, Groningen, Netherlands

<sup>6</sup>Department of Cardiology, Erasmus University Medical Center, University of Rotterdam, Rotterdam, Netherlands

## Correspondence

Francesco Lodola and Antonio Zaza, Department of Biotechnology and Bioscience, University of Milano-Bicocca, P.za della Scienza 2, Milan 20126, Italy. Email: [francesco.lodola@unimib.it](mailto:francesco.lodola@unimib.it) and [antonio.zaza@unimib.it](mailto:antonio.zaza@unimib.it)

## Funding information

Generation of the PLN-R14del murine model was supported by grants from the Netherlands Heart Foundation (CVON PREDICT2, Grant/award: 2018-30; CVON DOUBLE DOSE, Grant/award: 2020B005 and CarMa, Grant/award:01-003-2022-0358).

## Abstract

**Aims:** The heterozygous phospholamban (PLN) mutation R14del (PLN R14del<sup>+/-</sup>) is associated with a severe arrhythmogenic cardiomyopathy (ACM) developing in the adult. “Superinhibition” of SERCA2a by PLN R14del is widely assumed to underlie the pathogenesis, but alternative mechanisms such as abnormal energy metabolism have also been reported. This work aims to (1) to evaluate Ca<sup>2+</sup> dynamics and energy metabolism in a transgenic (TG) mouse model of the mutation prior to cardiomyopathy development; (2) to test whether they are causally connected.

**Methods:** Ca<sup>2+</sup> dynamics, energy metabolism parameters, reporters of mitochondrial integrity, energy, and redox homeostasis were measured in ventricular myocytes of 8–12 weeks-old, phenotypically silent, TG mice. Mutation effects were compared to pharmacological PLN antagonism and analyzed during modulation of sarcoplasmic reticulum (SR) and cytosolic Ca<sup>2+</sup> compartments. Transcripts and proteins of relevant signaling pathways were evaluated.

**Results:** The mutation was characterized by hyperdynamic Ca<sup>2+</sup> handling, compatible with a loss of SERCA2a inhibition by PLN. All components of energy metabolism were depressed; myocyte energy charge was preserved under quiescence but reduced during stimulation. Cytosolic Ca<sup>2+</sup> buffering or SERCA2a blockade reduced O<sub>2</sub> consumption with larger effect in the mutant. Signaling changes suggest cellular adaptation to perturbed Ca<sup>2+</sup> dynamics and response to stress.

**Conclusions:** (1) PLN R14del<sup>+/-</sup> loses its ability to inhibit SERCA2a, which argues against SERCA2a superinhibition as a pathogenetic mechanism; (2) depressed energy metabolism, its enhanced dependency on Ca<sup>2+</sup> and activation of signaling responses point to an early involvement of metabolic stress in the pathogenesis of this ACM model.

## KEYWORDS

arrhythmogenic cardiomyopathy, energy metabolism, phospholamban, PLN R14del<sup>+/-</sup>, PLN-SERCA2a interaction

Francesco Lodola and Antonio Zaza equally contributed to this work.

© 2024 Scandinavian Physiological Society. Published by John Wiley & Sons Ltd

## 1 | INTRODUCTION

Phospholamban (PLN) is a small protein which restrains SERCA2a operation, thus limiting  $\text{Ca}^{2+}$  uptake by the sarcoplasmic reticulum (SR) under resting conditions. Receptor triggered phosphorylation (e.g., by PKA) positively regulates SERCA2a by relieving inhibition by PLN.

The heterozygous deletion of arginine 14 in PLN (PLN R14del<sup>+/-</sup>) is associated with a form of arrhythmogenic dilated cardiomyopathy (ACM), characterized by PLN aggregate formation, myocardial fibrosis, and heart failure, with typical onset at middle age.<sup>1</sup> PLN R14del<sup>+/-</sup> is among the prevailing cardiomyopathy-related mutations, particularly in the Netherlands<sup>2</sup> and currently lacks a specific treatment. More than a decade ago, the pioneering work of Haghghi et al.<sup>3</sup> ascribed PLN R14del<sup>+/-</sup> phenotype to a “superinhibitory” effect on SERCA2a detected, in a heterologous expression system, as a decrease in sensitivity of pump function to  $\text{Ca}^{2+}$ . Several subsequent studies, inspired by this interpretation, provided more or less indirect support<sup>4-6</sup> but also conflicting results.<sup>7-9</sup> At any rate, even among the supporting studies, the mechanisms proposed to account for the superinhibitory effect were inconsistent and remain debated.

The “superinhibition” theory motivated us to test reversal of PLN R14del<sup>+/-</sup> phenotype by a recently developed compound (PST-3093) that selectively stimulates SERCA2a by antagonizing its interaction with PLN.<sup>10</sup> Unexpectedly, human iPS cardiomyocytes (hiPS-CMs), derived from a heterozygous human mutation carrier, displayed a hyperdynamic  $\text{Ca}^{2+}$  handling instead, a phenotype that is obviously incompatible with SERCA2a “superinhibition”. Notably, PST-3093 mimicked the effect of the mutation when applied to the WT hiPS-CMs, but was ineffective in mutant ones.<sup>11</sup> Studies on contracting engineered tissues (EHT), obtained from the same hiPS-CMs, detected a major decrease in force development and energy metabolism derangements, but no clear abnormalities in intracellular  $\text{Ca}^{2+}$  dynamics.<sup>12</sup> Nonetheless, being such studies based on immature cells from a single mutation carrier, caution is warranted in generalization of these results, particularly in light of the wide acceptance of the superinhibition hypothesis.

We have developed and characterized a PLN R14del<sup>+/-</sup> transgenic (TG) mouse model which closely recapitulates the human ACM phenotype, including lack of cardiac abnormalities at young age.<sup>13</sup> The present work characterizes cardiomyocytes (CMs) obtained from this disease model in terms of mutation effect on intracellular  $\text{Ca}^{2+}$  dynamics and energy metabolism. This with the aim of testing the “superinhibition” theory in native mature CMs and compare them to hiPS-CMs for metabolic derangements, thus providing cross-validation of experimental models of the disease.

Evaluation of primary pathogenetic mechanisms in mutations leading to contractile deficit is complicated by overlap with the etiology-unspecific maladaptive process induced by the deficit itself, in which SERCA2a loss of function dominates.<sup>14</sup> To minimize this potential confounder, we selected an animal age at which cardiac contraction is still normal in the PLN R14del<sup>+/-</sup> TG mice.<sup>13</sup>

## 2 | RESULTS

### 2.1 | SERCA2a ATPase activity

SERCA2a ATPase activity correlates with  $\text{Ca}^{2+}$  transport rate,<sup>15</sup> its measurement in myocardial homogenates provides direct information on the transporter function in a simplified (cell-free) system.  $\text{Ca}^{2+}$ -sensitivity of SERCA2a activity is mostly determined by SERCA2a-PLN interaction and is therefore suitable to detect its abnormalities.<sup>15</sup> In myocardial homogenate preparations, the  $\text{Ca}^{2+}$  dissociation constant [ $\text{Kd}_{\text{Ca}}$ ] of SERCA2a ATPase activity was 21% lower (unpaired Student's *t*-test,  $p=0.0005$ ) in Mut; the maximum velocity of SERCA2a ATPase activity was similar between Mut and WT preparations. Mut SERCA2a ATPase activity exceeded WT one above 300 nM  $\text{Ca}^{2+}$  (Figure 1).

This observation suggests reduced inhibition of SERCA2a by PLN in Mut preparations.

### 2.2 | Intracellular $\text{Ca}^{2+}$ dynamics

Next, we evaluated SERCA2a function in the context of an intact myocyte. To improve mechanistic interpretation of the mutation effect, studies with an agent known to increase SERCA2a function by preventing its interaction with PLN<sup>10</sup> were included. SERCA2a function may have different impact on intracellular  $\text{Ca}^{2+}$  dynamics at different heart rates; therefore, the rate-dependency of changes in  $\text{Ca}^{2+}$  dynamics was also evaluated in a separate set of CMs field-stimulated at four rates between 1 and 2 Hz. Since these experiments aim to compare the rate-dependency of effect, statistical significance refers to the Treatment  $\times$  Rate interaction.

#### 2.2.1 | Effect of the mutation

##### *Steady-state stimulation (1 Hz)*

Mut effect on intracellular  $\text{Ca}^{2+}$  dynamics was assessed in intact WT and Mut CMs during steady-state field-stimulation at 1 Hz (Figure 2).  $\text{Ca}^{2+}$  transient ( $\text{CaT}$ ) parameters were measured as described in Section 5. In Mut CMs  $\tau_{\text{decay}}$  (Figure 2E) was shorter by 43% (Mann-Whitney *U*-test,  $p<0.0001$  vs. WT), diastolic  $\text{Ca}^{2+}$  ( $\text{CaD}$ , Figure 2F) was 5% lower

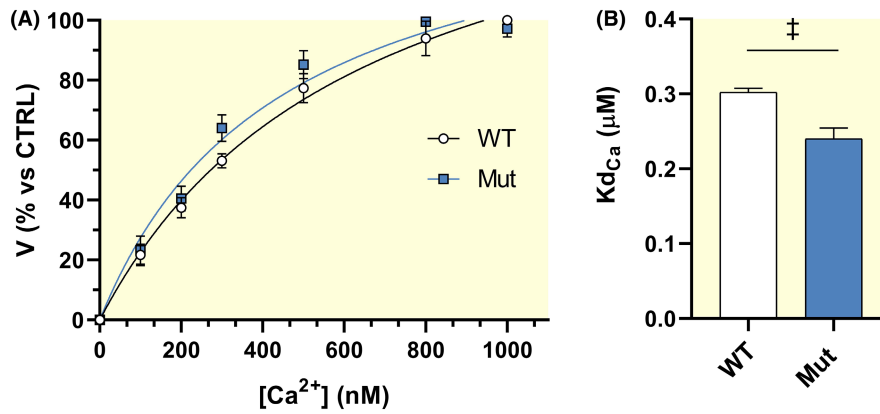
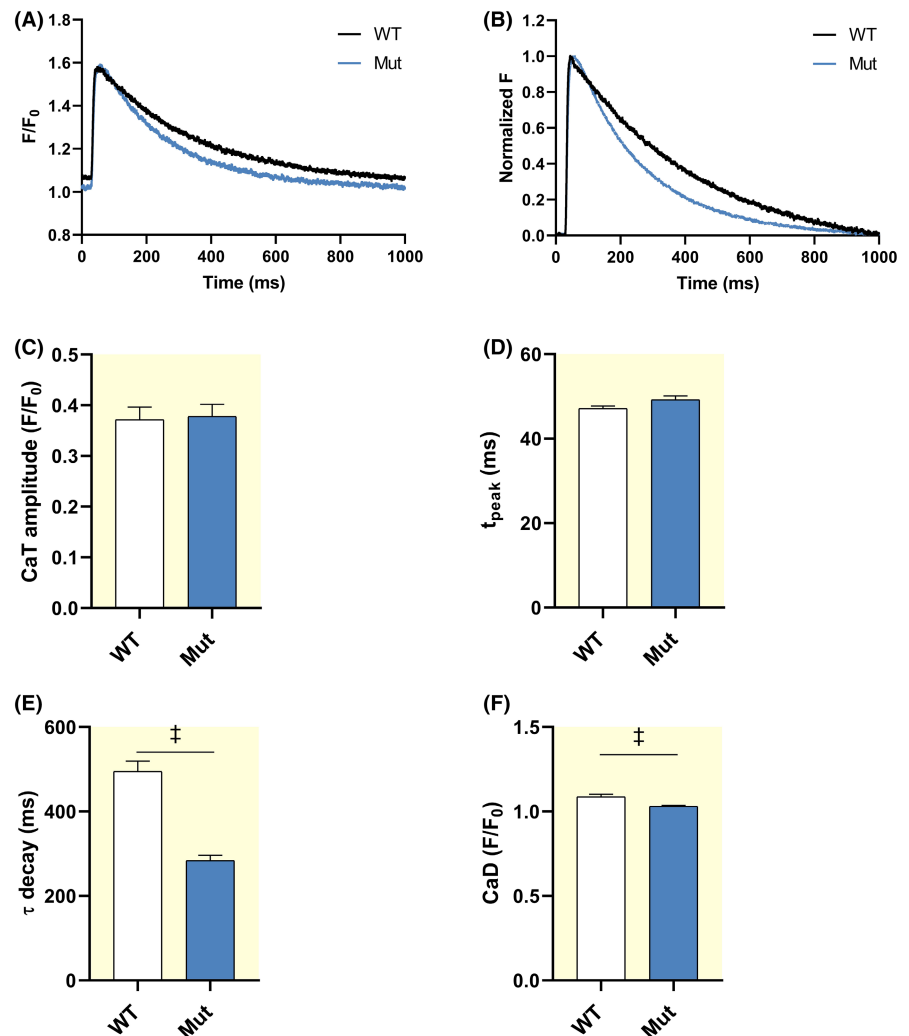


**FIGURE 1**  $\text{Ca}^{2+}$ -dependent activation of SERCA2a ATPase in ventricular homogenates. (A) SERCA2a (CPA-sensitive) ATPase activity as function of medium  $\text{Ca}^{2+}$  concentration; solid lines obtained by fitting with Hill functions. (B)  $\text{Ca}^{2+}$  dissociation constant ( $K_{d\text{Ca}}$ , lower values reflect increased affinity) estimated from the fitting (WT:  $0.30 \pm 0.01$ ,  $n = 10$ ; Mut:  $0.24 \pm 0.01$ ,  $n = 8$ ). WT:  $N = 2$  preparations (4–5 technical replicates each); Mut:  $N = 2$  preparations (4 technical replicates each). Data are expressed as mean  $\pm$  SEM. Unpaired Student's  $t$ -test.

**FIGURE 2** Parameters of calcium transients. (A) Representative  $\text{Ca}^{2+}$  transients (CaT). (B) CaT normalized to peak amplitude to illustrate changes in kinetics. (C) CaT amplitude (WT:  $0.37 \pm 0.03$ ,  $n = 32$ ; Mut:  $0.38 \pm 0.02$ ,  $n = 27$ ). (D) CaT time to peak,  $t_{\text{peak}}$  (WT:  $47.1 \pm 0.56$ ,  $n = 30$ ; Mut:  $49.2 \pm 0.94$ ,  $n = 27$ ). (E)  $\text{Ca}^{2+}$  transient decay kinetics,  $\tau_{\text{decay}}$  (WT:  $495 \pm 24.1$ ,  $n = 32$ ; Mut:  $284 \pm 12.2$ ,  $n = 27$ ). (F) Diastolic  $\text{Ca}^{2+}$ , CaD (WT:  $1.09 \pm 0.02$ ,  $n = 31$ ; Mut:  $1.03 \pm 0.01$ ,  $n = 27$ ). WT:  $N = 4$ ; Mut:  $N = 4$ . Data expressed as mean  $\pm$  SEM;  $p$  by Mann–Whitney  $U$ -test.



(Mann–Whitney  $U$ -test,  $p = 0.0002$  vs. WT) and remarkably less variable. CaT amplitude (Figure 2C) and rise-time ( $t_{\text{peak}}$ , Figure 2D) were comparable between the two genotypes.

#### Rate-dependency

The following CaT parameters showed significant rate-dependency in WT CMs (Figure S1):  $t_{\text{peak}}$  (inverse,

$p < 0.0001$ ),  $\tau_{\text{decay}}$  (inverse,  $p < 0.0001$ ), CaD (direct,  $p < 0.0001$ ).

As compared to WT, in Mut CMs:  $\tau_{\text{decay}}$  had a shallower rate-dependency (Figure S1C, Mixed-effects model, Treatment  $\times$  Rate,  $p = 0.0015$  vs. WT) due to preferential shortening at slow rates. As expected from faster SR  $\text{Ca}^{2+}$  uptake, CaD accumulation was less pronounced in Mut CMs (Figure S1D, Mixed-effects model, Treatment  $\times$  Rate,  $p = 0.0114$  vs. WT).

For the remaining parameters, rate dependency was similar between the two genotypes.

#### SR reloading rate and steady-state SR $\text{Ca}^{2+}$ content

SR  $\text{Ca}^{2+}$  uptake function was assessed in V-clamped CMs by the “SR reloading” protocol and by measuring caffeine-releasable SR  $\text{Ca}^{2+}$  content (CaSR) (Figure 3A, see Section 5). The difference between Mut and WT CMs in the behavior of CaT parameters during SR reloading (from step 1 to 15) is reported below (Figure 3).

CaT amplitude progressively increased during SR reloading, as expected (Figure 3C). The rate of such increment, as well as the final amplitude value, were larger for Mut CMs (Mixed-effects model, Treatment  $\times$  Step,  $p < 0.0001$  vs. WT). The same pattern was observed after CaT normalization for  $\text{Ca}^{2+}$  influx through  $I_{\text{CaL}}$  (Figure 3F, CICR gain); however, because of the larger variance in Mut data, for this parameter statistical significance was not achieved.

The  $\tau_{\text{decay}}$  progressively decreased during SR reloading (Figure 3D). In Mut CMs it started off from considerably lower values, but its progressive decline over the protocol was shallower (Mixed-effects model, Treatment  $\times$  Step,  $p < 0.0001$  vs. WT). CaD started off from a lower value in Mut CMs (unpaired Student's  $t$ -test,  $p = 0.0085$ ), but the difference decreased thereafter (Figure 3E, Mixed-effects model, Treatment  $\times$  Step,  $p = 0.0061$  vs. WT).

Under the conditions of this experiment, SR  $\text{Ca}^{2+}$  content (CaSR) was considerably larger in Mut CMs (Figure 3H, unpaired Student's  $t$ -test,  $p = 0.0003$  vs. WT); fractional release was similar between Mut and WT CMs (Figure 3I).

To summarize, as compared to WT ones, Mut CMs were characterized by “hyperdynamic”  $\text{Ca}^{2+}$  handling, compatible with loss of SERCA2a inhibition (as opposed to enhanced inhibition). This pattern was consistent between

CaT parameters of intact CMs during field-stimulation and evaluation of SR reloading under V-clamp.

#### NCX “conductance” and equilibrium

NCX functional parameters were measured during the caffeine pulse, that is under conditions short-circuiting SR transports (Figure S2).

In Mut CMs NCX “conductance” was significantly decreased (Figure S2B, Mann–Whitney  $U$ -test,  $p = 0.02$  vs. WT);  $\text{Ca}^{2+}$  concentration at the (extrapolated) 0  $I_{\text{NCX}}$  value (transport equilibrium point) was not significantly changed (Figure S2C).

### 2.2.2 | Effect of PLN antagonism (PST-3093) in MUT versus WT CMs

#### Steady state stimulation (1 Hz)

The effect of PLN antagonism by PST-3093 on intracellular  $\text{Ca}^{2+}$  dynamics was assessed in intact WT and Mut CMs during steady-state field-stimulation at 1 Hz. CaT parameters were measured as described in the Section 5.

In WT CMs, PST-3093 reduced  $\tau_{\text{decay}}$  by 24% (Figure S3E, One-way ANOVA, post-hoc  $p = 0.0209$  vs. Control); the remaining parameters were unaffected (Figure S3).

In Mut CMs, PST-3093 failed to affect the CaT parameters significantly (Figure S3), notably including  $\tau_{\text{decay}}$  (Figure S3E).

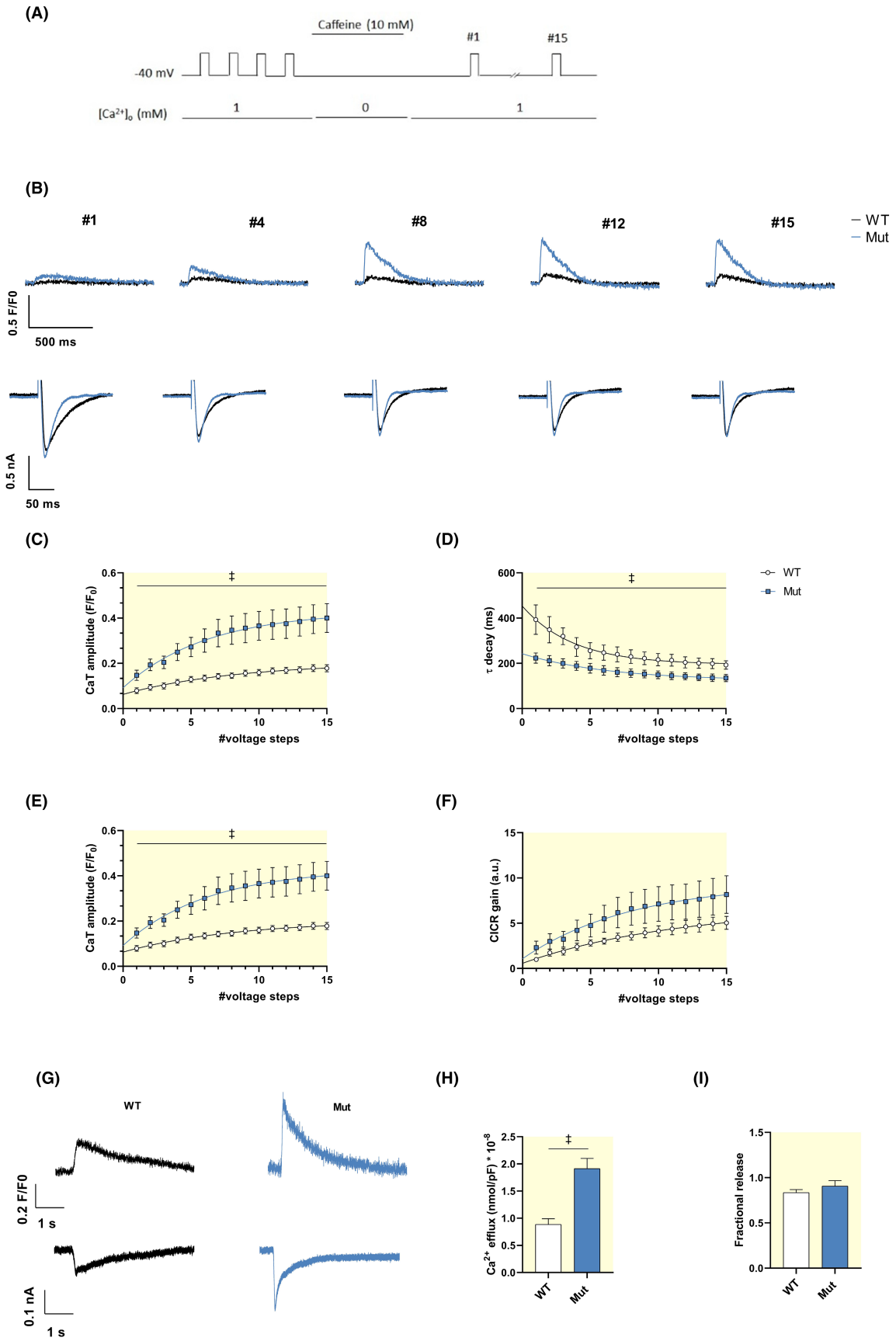
#### Rate dependency

For both WT and Mut CMs, CaT parameters showing significant rate dependency (direct or inverse) under control conditions were:  $t_{\text{peak}}$  (inverse,  $p < 0.0001$ ),  $\tau_{\text{decay}}$  (inverse,  $p < 0.0001$ ) and CaD (direct,  $p < 0.0001$ ) (Figures S4 and S5).

In Mut CMs, PST-3093 enhanced rate-dependent accumulation of CaD (Figure S5D, Mixed-effects model, Treatment  $\times$  Rate,  $p = 0.004$  vs. Control). Rate dependency of all the remaining parameters was not significantly affected by PST-3093 in both genotypes (Figures S4 and S5).

To summarize, in WT CMs PST-3093 had, as postulated, effects compatible with SERCA2a activation (hyperdynamic  $\text{Ca}^{2+}$  handling), although quantitatively smaller than those exerted by the mutation. On the

**FIGURE 3** SR  $\text{Ca}^{2+}$  uptake and content. (A) Experimental protocol. (B) Representative  $\text{Ca}^{2+}$  transients (CaT, upper panels) and voltage-dependent calcium currents ( $I_{\text{CaL}}$ ) (lower panels) recorded during SR reloading after caffeine-induced depletion. WT (black) and Mut (green) traces are superimposed for comparison. (C–F) Mean values of CaT parameters measured during each voltage step (1–15) of the loading train. WT:  $n = 9$ ,  $N = 7$ ; Mut:  $n = 11$ ,  $N = 6$ ;  $p$  by Mixed-effects ANOVA for loading rate. (G) Representative traces of  $\text{Ca}^{2+}$  transients (upper panels) and membrane currents,  $I_{\text{m}}$  (lower panels) recorded during caffeine-induced SR release. (H) SR  $\text{Ca}^{2+}$  content (CaSR) estimated from the integral of  $I_{\text{m}}$  (representative of  $I_{\text{NCX}}$ ) (WT:  $0.89 \pm 0.11$ ,  $n = 9$ ; Mut:  $1.91 \pm 0.19$ ,  $n = 11$ ). (I) Fractional SR  $\text{Ca}^{2+}$  release (WT:  $0.83 \pm 0.04$ ,  $n = 9$ ; Mut:  $0.91 \pm 0.06$ ,  $n = 11$ ). WT:  $N = 7$ ; Mut:  $N = 6$ . Data expressed as mean  $\pm$  SEM;  $p$  by unpaired Student's  $t$ -test.



other hand, PST-3093 effects were nil, or even opposite, in Mut CMs.

## 2.3 | Energy metabolism

Derangement of mitochondrial function is a common feature of the (secondary) “remodeling” process and is related to mishandling of intracellular  $\text{Ca}^{2+}$  and it ultimately contributes to the development of heart failure. The aim of this set of experiments was to test whether the energy metabolism was altered in Mut CMs at a stage preceding overt contractile failure, thus possibly acting as a primary pathogenetic factor instead. Notably, because of technical constraints, metabolic measurements were performed in unstimulated (quiescent) CMs.

### 2.3.1 | Oxygen consumption rate

$\text{O}_2$  consumption rate (OCR) was compared between quiescent WT and Mut CMs within the same multiwell plate (Figure 4). OCR values were normalized for the number of cells in each well. Mitochondrial respiration profile, from which the respiration parameters were derived, was obtained by modulating specific functions with pharmacological agents, as described in the Section 5. The pattern observed in Mut CMs is reported below as relative to that of WT ones.

Overall, OCR was significantly depressed in Mut CMs (Figure 4A); the observation was reproduced with remarkable consistency across all the preparations tested. The largest difference was found in maximal OCR (Figure 4C,  $-36\%$ ; Mann–Whitney  $U$ -test,  $p < 0.0001$ ); nonetheless, basal OCR (Figure 4B,  $-39\%$ ; unpaired Student's  $t$ -test,  $p = 0.0006$ ) and spare respiratory capacity (Figure 4D,  $-35\%$ ; Mann–Whitney  $U$ -test,  $p < 0.0001$ ) were also reduced. Notably, significantly lower values were also found for the non-mitochondrial component of OCR (Figure 4E,  $-38\%$ ; unpaired Student's  $t$ -test,  $p = 0.0003$ ).

Modulation of OCR by cytosolic  $\text{Ca}^{2+}$ , and by the SR compartment specifically, was evaluated in a subset of samples. To this end, cytosolic  $\text{Ca}^{2+}$  was chelated by BAPTA-AM (BAPTA) (Figure 5A,B,C,E) and SERCA2a was inhibited by thapsigargin (THAPSI) incubation, thus functionally removing the SR contribution (Figure 5A,B,D,F). Both interventions depressed basal OCR, though, THAPSI effect did not differ significantly between WT and Mut CMs (Figure 5 middle panels). Maximal OCR was instead unaffected by THAPSI in WT CMs, but significantly depressed in Mut ones (Figure 5 bottom panels). There was no obvious difference between BAPTA and THAPSI

effects on OCR. The drugs vehicle (DMSO) unexpectedly increased OCR in Mut myocytes only. Nonetheless, the same DMSO concentration was present across the experimental groups; therefore, this effect does not impact on the evaluation of BAPTA and THAPSI effect.

### 2.3.2 | Glycolysis

Anaerobic glycolytic metabolism was evaluated, in the same plates subjected to OCR measurements, as proton efflux rate (PER) (Figure 6). PER values were normalized for the number of cells in the wells of the Seahorse plate. PER was measured under basal conditions, after inhibiting mitochondrial respiration (by Rotenone/Antimycin A) to assess compensatory glycolysis, and after blocking glycolysis by 2-deoxy-D-glucose (2DG) to assess non-glycolytic acidification.

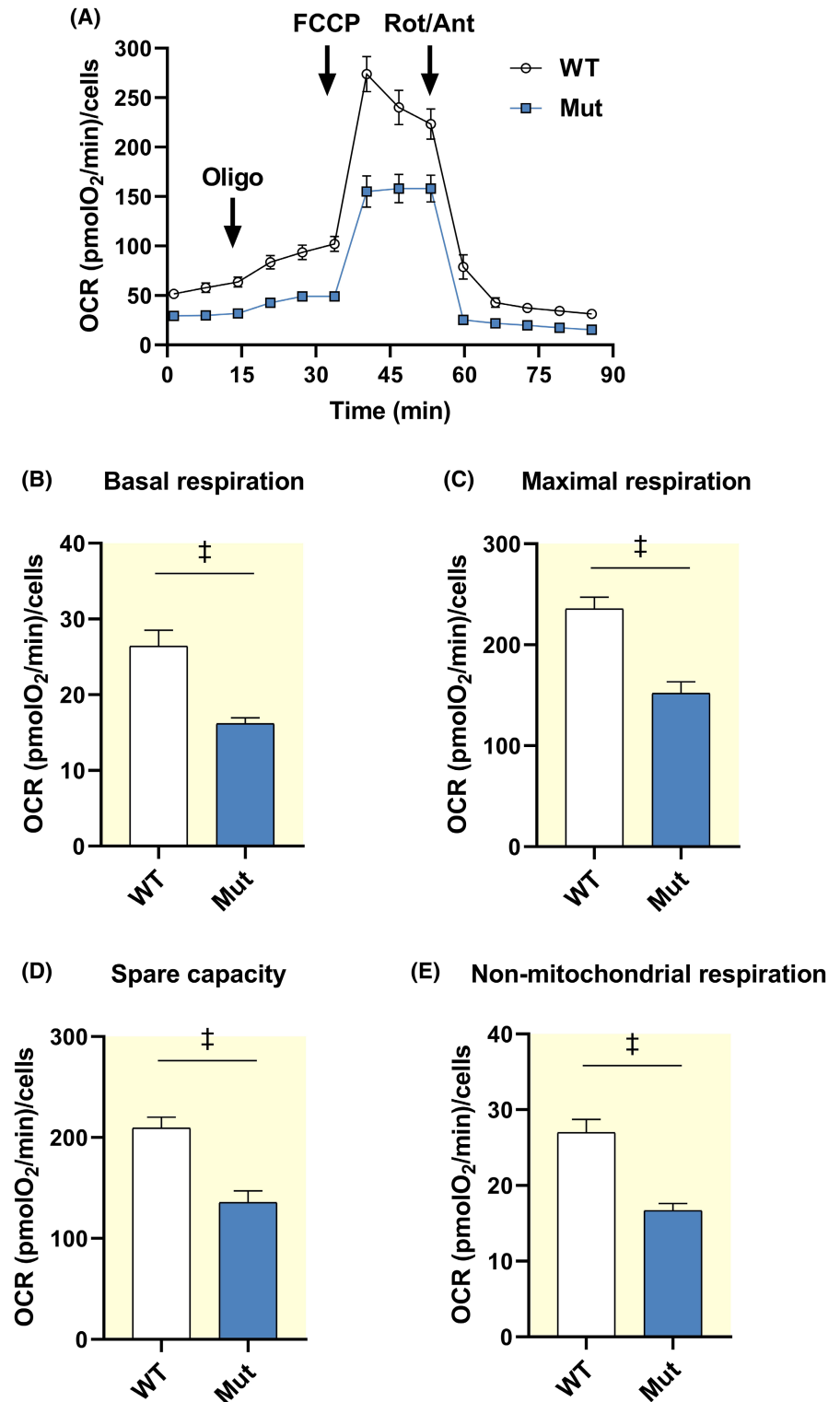
Anaerobic glycolysis was depressed in Mut CMs as compared to WT ones (Figure 6A). While basal glycolysis showed only a trend to reduction (Figure 6B,  $-23\%$ ; unpaired  $t$ -test,  $p = 0.0882$ ), compensatory glycolysis (Figure 6C,  $-47\%$ ; unpaired Student's  $t$ -test,  $p = 0.0005$ ) and glycolytic reserve (Figure 6D,  $-58\%$ ; unpaired Student's  $t$ -test,  $p = 0.0015$ ) were severely depressed. Non-glycolytic acidification was slightly ( $-23\%$ ), but still significantly, reduced (Figure 6E, Mann–Whitney  $U$ -test,  $p = 0.0089$ ).

### 2.3.3 | Cell energy charge

To assess whether the reduction in energy metabolism of Mut CMs leads to energy starvation, we measured the current carried by the glibenclamide-sensitive  $\text{K}^+$  channel ( $I_{\text{KATP}}$ ), whose conductance is sensitive to the ADP/ATP ratio.<sup>16</sup> This surrogate measurement (validation reported in Figure S6B) was adopted because, in preliminary experiments, we found bulk fluorescence ATP assays to be confounded by unusually large number of dead CMs in the preparations (see Figure S6A). To avoid intracellular dialysis by the pipette content, measurements were performed with the perforated-patch technique.  $I_{\text{KATP}}$  was recorded at  $-120$  mV, membrane potential at which  $\text{K}^+$  currents are expectedly inward (i.e., a positive current shift reflects a decrease in  $I_{\text{KATP}}$ ).  $I_{\text{KATP}}$  was normalized to membrane capacitance to obtain current density.

Under quiescence, no significant difference in mean  $I_{\text{KATP}}$  density was observed between WT and Mut CMs; nonetheless, very large  $I_{\text{KATP}}$  values were occasionally recorded in Mut CMs (Figure 7A,B). Immediately after stimulation, mean  $I_{\text{KATP}}$  density was approximately 3-fold larger in Mut CMs than in WT ones (Figure 7C,D).

**FIGURE 4** Parameters of mitochondrial respiration. (A) Oxygen consumption rate (OCR) profiles of WT and Mut CMs subjected to sequential injections of 1.5  $\mu$ M Oligo, 0.5  $\mu$ M FCCP and 3  $\mu$ M Rot/Ant A (XF Mito Stress Test protocol). (B) Basal OCR (WT:  $26.40 \pm 2.13$ ,  $n = 31$ ; Mut:  $16.20 \pm 0.76$ ,  $n = 19$ ). (C) Maximal OCR (WT:  $235 \pm 11.46$ ,  $n = 31$ ; Mut:  $151 \pm 11.54$ ,  $n = 19$ ). (D) Spare respiratory capacity ( $209 \pm 10.76$ ,  $n = 31$ ; Mut:  $129 \pm 12.6$ ,  $n = 17$ ). (E) Non-mitochondrial OCR (WT:  $26.97 \pm 1.74$ ,  $n = 31$ ; Mut:  $16.68 \pm 0.94$ ,  $n = 19$ ). WT:  $N = 3$ ; Mut:  $N = 3$ . Data are expressed as mean  $\pm$  SEM;  $p$  by unpaired Student's  $t$ -test and Mann-Whitney  $U$ -test.



### 2.3.4 | Intracellular ROS and mitochondrial membrane potential ( $\Psi_m$ )

Intracellular radical oxygen species (ROS) content was estimated in quiescent CMs by measuring 2',7'-dichlorofluorescein diacetate (DCFDA) fluorescence; confocal images were automatically analyzed to quantify the signal from individual vital cells. In Mut CMs,

DCFDA signal was marginally, but significantly, lower than in WT CMs (Figure S7A,  $-5\%$ ; unpaired Student's  $t$ -test,  $p = 0.0115$  vs. WT), to indicate a slight reduction in ROS content.

Mitochondrial membrane potential ( $\Psi_m$ ) was evaluated by the fluorescent probe tetramethylrhodamine, ethyl ester (TMRE). TMRE signal was similar between Mut and WT CMs (Figure S7B). In the same CMs of both groups,

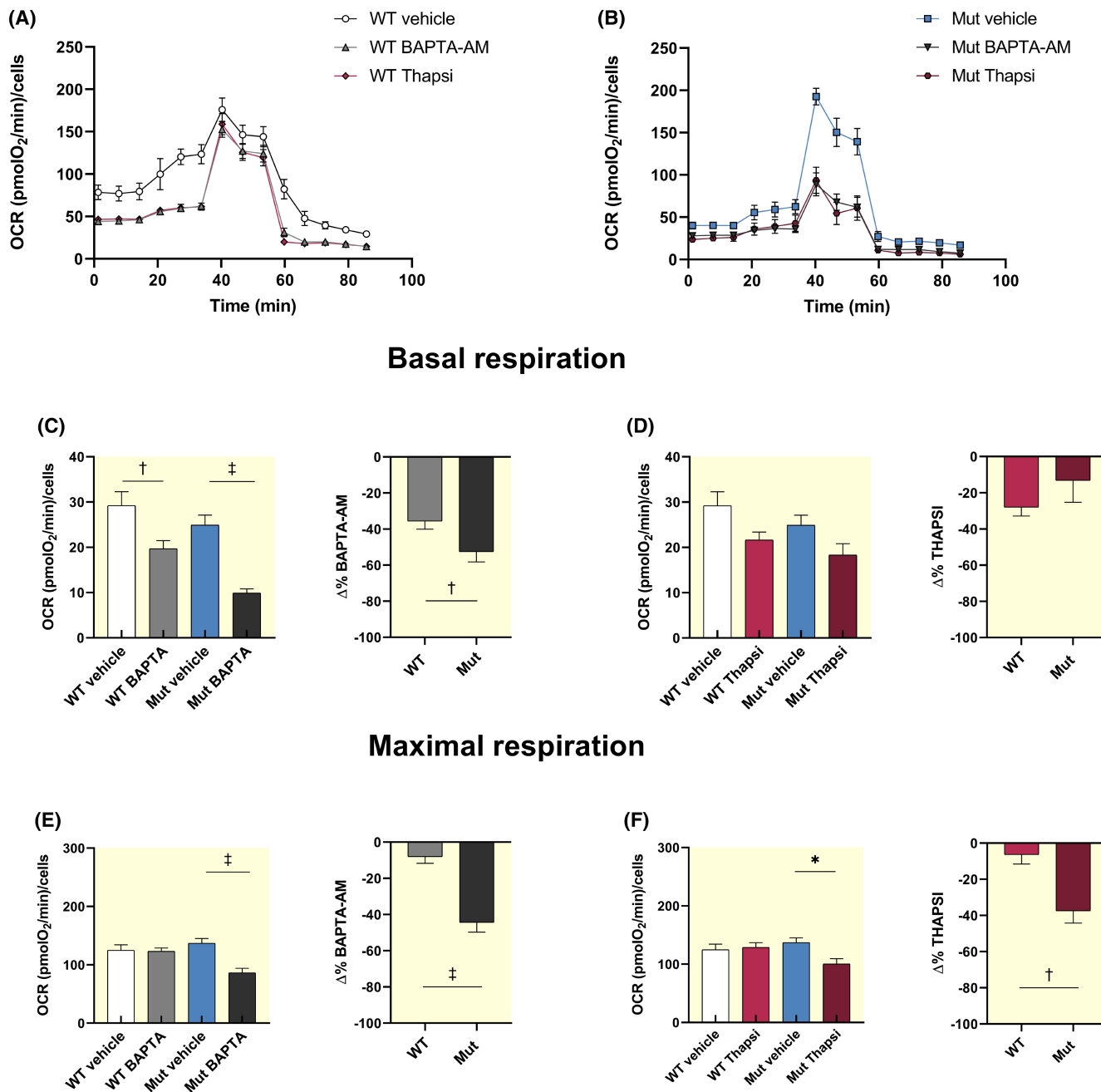


**FIGURE 5** Effect of BAPTA-AM and Thapsigargin on oxygen consumption rate (OCR). (A, B) OCR profiles of WT and Mut CMs (protocol as in Figure 4) treated with BAPTA-AM (BAPTA, 5  $\mu$ M) or thapsigargin (THAPSI, 5  $\mu$ M). (C, D) Treatment Effect on basal OCR (WT vehicle:  $29.22 \pm 3.04$ ,  $n = 19$  wells; WT BAPTA:  $19.69 \pm 1.79$ ,  $n = 35$  wells; Mut vehicle:  $24.92 \pm 2.20$ ,  $n = 15$  wells; Mut BAPTA:  $9.89 \pm 0.93$ ,  $n = 26$  wells); (WT vehicle:  $29.22 \pm 3.04$ ,  $n = 19$  wells; WT THAPSI:  $21.67 \pm 1.71$ ,  $n = 30$  wells; Mut vehicle:  $24.92 \pm 2.20$ ,  $n = 15$  wells; Mut THAPSI:  $18.32 \pm 2.51$ ,  $n = 24$  wells). (E, F) Treatment effect on maximal OCR (WT vehicle:  $125 \pm 9.42$ ,  $n = 18$  wells; WT BAPTA:  $123 \pm 5.61$ ,  $n = 35$  wells; Mut vehicle:  $137 \pm 8.00$ ,  $n = 15$  wells; Mut BAPTA:  $86.43 \pm 7.63$ ,  $n = 27$  wells); (WT vehicle:  $125 \pm 9.42$ ,  $n = 18$  wells; WT THAPSI:  $129 \pm 7.97$ ,  $n = 31$  wells; Mut vehicle:  $137 \pm 8.00$ ,  $n = 15$  wells; Mut THAPSI:  $100 \pm 9.08$ ,  $n = 24$  wells). WT:  $N = 3$ ; Mut:  $N = 3$ . Data are expressed as mean  $\pm$  SEM. One-way ANOVA and Kruskal–Wallis test for % data.

short-circuit of mitochondrial membrane by FCCP significantly increased TMRE signal, thus confirming responsiveness of the probe to  $\Psi_m$  changes (Figure S7B-inset).

To summarize, despite the absence of overt mitochondrial damage (normal ROS content and membrane polarization), both the oxidative and anaerobic components of

energy metabolism were depressed in Mut CMs. While OCR was clearly sensitive to interventions affecting cytosolic  $\text{Ca}^{2+}$ , only the response of maximal OCR differed between WT and Mut CMs. A defect in cell energy charge of Mut CMs, undetectable under quiescence, was clearly uncovered by stimulation.



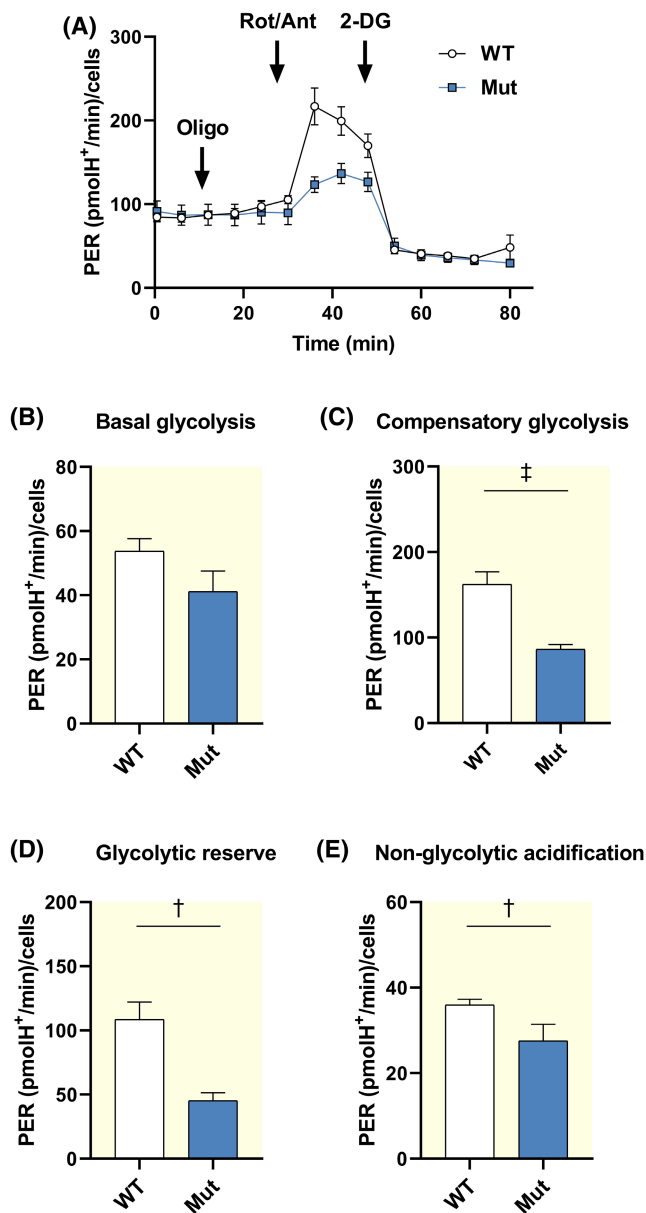


**FIGURE 6** Parameters of anaerobic glycolysis. (A) Proton efflux rate (PER) profile of WT and Mut CMs subjected to sequential injections of 1.5  $\mu$ M Oligo, 3  $\mu$ M Rot/Ant and 50 mM 2-DG. (B) Basal glycolysis (WT:  $53.77 \pm 3.84$ ,  $n = 13$ ; Mut:  $41.15 \pm 6.42$ ,  $n = 9$ ). (C) Compensatory glycolysis (WT:  $162 \pm 14.52$ ,  $n = 13$ ; Mut:  $86.34 \pm 5.48$ ,  $n = 9$ ). (D) Glycolytic reserve (WT:  $109 \pm 13.58$ ,  $n = 13$ ; Mut:  $45.19 \pm 6.23$ ,  $n = 9$ ). (E) Non-glycolytic acidification (WT:  $36 \pm 1.29$ ,  $n = 13$ ; Mut:  $27.56 \pm 3.84$ ,  $n = 9$ ). WT:  $N = 3$ ; Mut:  $N = 3$ . Data expressed as mean  $\pm$  SEM;  $p$  by unpaired Student's  $t$ -test or Mann-Whitney  $U$ -test.

## 2.4 | Transcript and protein analysis

The functional derangements reported above may suggest profound changes in Mut CMs biology, may they depend on altered  $\text{Ca}^{2+}$  handling, or on direct toxicity of mutated PLN. In a broad, but focused, attempt to identify specific processes involved in the overall cell response to

the mutation, we analyzed transcriptional expression of elements clustering in the following functional groups: (1) remodeling of mitochondria (Mitophagy) and their SR contact sites (MERCs); (2) antioxidant response (DETOX); (3) response to energy starvation (AMPK); (4) response to ER stress (UPR); (5) CaMKII signaling (Figure S8). Western blots were obtained for pErk/Erk (Figure 8A), Bax (Figure 8B), IP<sub>3</sub>R, pAMPK/AMPK (Figure 8C), pCaMKII/CaMKII (Figure 8D) and SERCA2 (Figure 8E).

The transcription of genes involved in UPR and mitophagy were unchanged (Figure S8). Nonetheless, a trend to activation of signals involved in the response to ER-stress (pErk/Erk and Bax) was observed at the protein level (Figure 8A,B).

Genes encoding a couple of AMPK isoforms were up-regulated by 1.5–2 fold (Figure S8); however, the pAMPK/AMPK protein ratio showed, if anything, a trend to decrease, thus arguing against activation of energy starvation signaling, at least under quiescence (Figure 8C).

Genes encoding IP<sub>3</sub>R were unchanged (Figure S8); nonetheless, IP<sub>3</sub>R protein level was significantly increased (Figure 8C), perhaps as a compensation to increased OCR dependency on  $\text{Ca}^{2+}$  (see Figure 5).<sup>12</sup>

Genes encoding CaMKII were unchanged; moreover, at protein level, the pCaMKII/CaMKII ratio was not increased (Figure 8D). Thus, CaMKII signaling may not be activated at this disease stage.

Albeit failing to achieve statistical significance, SERCA2 expression showed a trend to increase in Mut myocardium (Figure 8E).

To summarize, transcript and protein analysis mainly led to negative conclusions regarding activation of energy starvation, CaMKII signaling or ROS detoxification. The few positive results hint to activation of ER-stress response and perturbed functional interaction between SR and mitochondria.

## 3 | DISCUSSION

The main findings of this study are as follows. As compared to WT ones, Mut hearts were characterized by (1) a lower  $K_{d_{\text{Ca}}}$  (higher  $\text{Ca}^{2+}$  affinity) of SERCA2a ATPase activity (Figure 1B); (2) intracellular  $\text{Ca}^{2+}$  dynamics compatible with enhanced SR  $\text{Ca}^{2+}$  uptake (Figure 2); (3) insensitivity of  $\text{Ca}^{2+}$  dynamics to PLN antagonism by PST-3093 (Figures S3–S5); (4) lower NCX conductance (Figure S2). All these findings point to diminished SERCA2a inhibition by Mut PLN, resulting in increased  $\text{Ca}^{2+}$  cycling by the pump. These changes in intracellular  $\text{Ca}^{2+}$  handling were accompanied by an overall depression of energy metabolism, consisting in a parallel reduction of OCR and anaerobic glycolysis (Figures 4

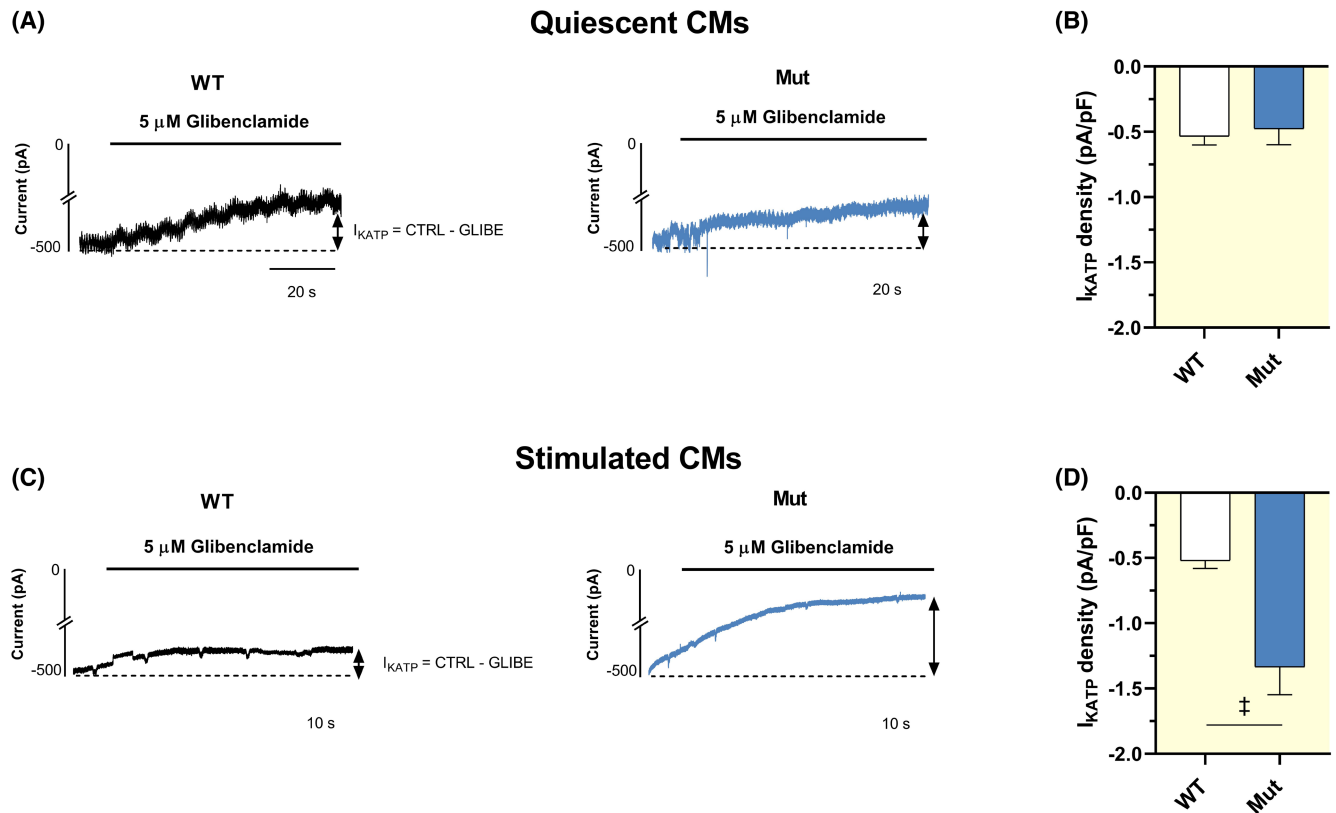


**FIGURE 7** Energy charge in quiescent and paced CMs. Energy charge was estimated from the conductance of ATP-sensitive  $\text{K}^+$  current ( $I_{\text{KATP}}$ ), which is proportional to the ADP/ATP ratio. (A) Representative current traces recorded in quiescent CMs (holding potential  $-120\text{ mV}$ ), in control conditions and during perfusion with  $5\ \mu\text{M}$  glibenclamide;  $I_{\text{KATP}}$  was calculated as the current difference (control – glibe) normalized to membrane capacitance to obtain current density. (B) Statistics of  $I_{\text{KATP}}$  density in quiescent CMs (WT:  $-0.53 \pm 0.07$ ,  $n=9$ ; Mut:  $-0.47 \pm 0.12$ ,  $n=8$ ). WT:  $N=7$ ; Mut:  $N=6$ . (C) Representative current traces recorded after pacing (2 Hz) in control conditions and during perfusion with  $5\ \mu\text{M}$  glibenclamide. (D) Statistics of  $I_{\text{KATP}}$  density after pacing (WT:  $-0.52 \pm 0.06$ ,  $n=12$ ; Mut:  $-1.34 \pm 0.21$ ,  $n=10$ ). WT:  $N=3$ ; Mut:  $N=4$ . Data expressed as mean  $\pm$  SEM;  $p$  by unpaired Student's  $t$ -test.

and 6). Despite the apparent oxidative impairment, ROS content and mitochondrial membrane polarization were remarkably normal in Mut CMs (Figure S7). The  $\text{Ca}^{2+}$ -dependency of maximal OCR was increased in Mut CMs (Figure 5). Under quiescence, cell energy charge and energy starvation signaling (pAMPK/AMPK) were unperturbed (Figure 8); nonetheless, the pacing-induced reduction of cell energy charge was larger in Mut CMs (Figure 7).

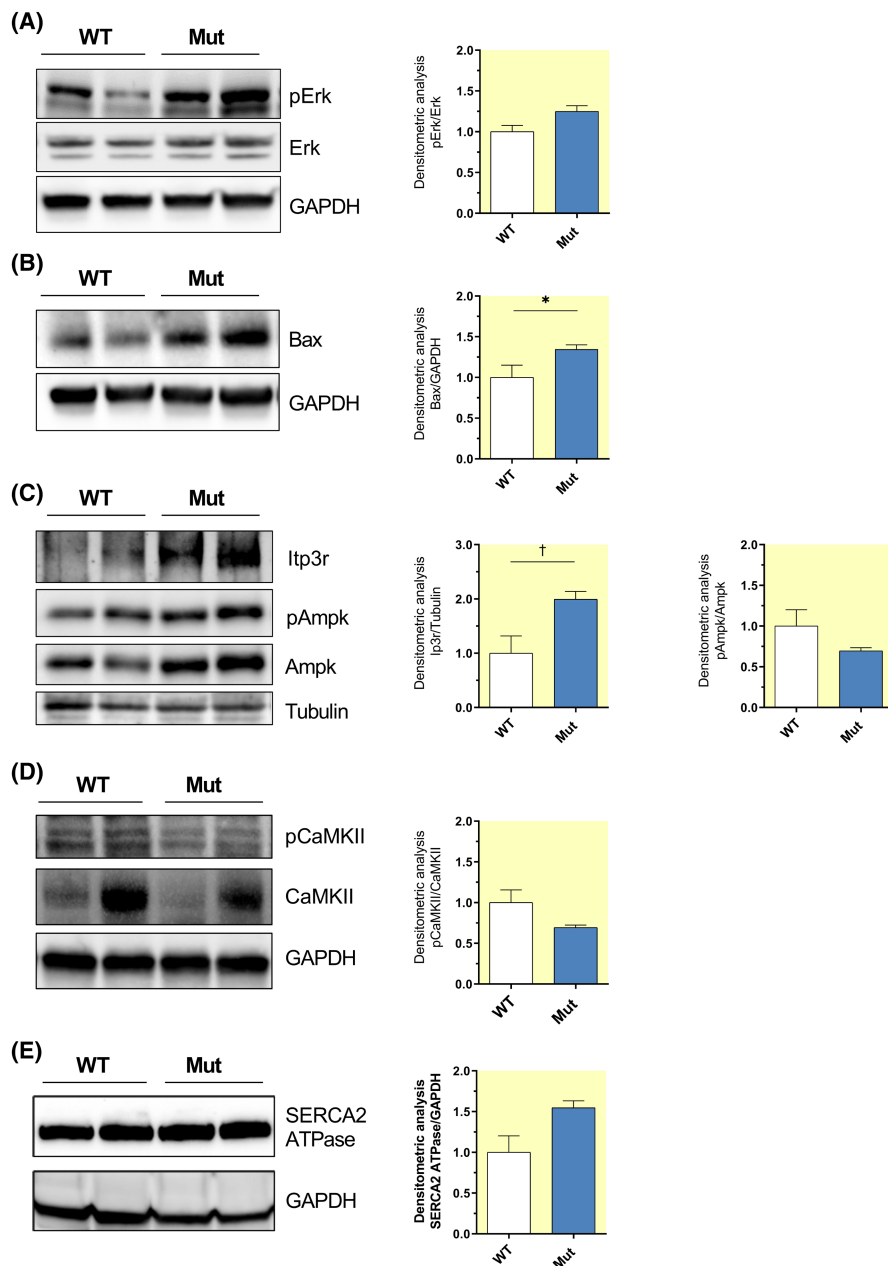
### 3.1 | Intracellular $\text{Ca}^{2+}$ dynamics

The mutation-associated changes in the parameters describing intracellular  $\text{Ca}^{2+}$  dynamics of intact CMs confirm the hyperdynamic state we observed in hiPS-CMs of a patient carrying the PLN-R14del mutation,<sup>11</sup> thus allowing generalization of that observation. The view that hyperdynamic  $\text{Ca}^{2+}$  handling reflects enhanced SERCA2a activity is reinforced by (1) increased  $\text{Ca}^{2+}$  sensitivity (lower  $\text{Kd}_{\text{Ca}}$ ) of SERCA2a ATPase activity

in myocardial homogenates; (2) similarity with the effect of PST-3093, a SERCA2a stimulator. The latter is known to increase SERCA2a activity by weakening its interaction with PLN,<sup>10</sup> thus suggesting reduced affinity for SERCA2a as a mechanism of PLN R14del behavior. In the PLN R14del heterozygous state, PST-3093 should have retained part of its stimulatory effect by displacing residual WT PLN. However, both in the PLN-R14del mouse (present study) and in heterozygous PLN R14del<sup>+/-</sup> patient-derived hiPS-CMs,<sup>11</sup> PST-3093 lost its SERCA2a stimulating effect completely (Figures S3–S5). This may suggest negative dominance of the mutation, one putative mechanism being enhanced PLN trapping in the non-inhibitory pentameric form.<sup>17</sup>

The hyperdynamic  $\text{Ca}^{2+}$  handling observed in the present study contrasts with the depressed  $\text{Ca}^{2+}$  handling reported in a heterozygous PLN R14del mouse based on knock-in of human PLN genes.<sup>18,19</sup> The development of cardiac abnormalities has a rather different time-course in the two models: whereas in the former signs of depressed contractility appear at 18–20 months of age,<sup>13</sup> clear-cut

**FIGURE 8** Protein analysis in myocardial homogenates. *Left panels:* representative Western Blots of proteins extracted from RV samples of WT and Mut mice (GAPDH or Tubulin included as housekeeping for normalization); *Right panels:* blot quantification by densitometric analysis normalized to housekeeping. (A) Erk and pErk (WT:  $1.0000 \pm 0.0777$ ,  $N=4$ ; Mut:  $1.2493 \pm 0.0691$ ,  $N=4$ ). (B) Bax (WT:  $1.0000 \pm 0.1506$ ,  $N=5$ ; Mut:  $1.3475 \pm 0.0529$ ,  $N=8$ ). (C) Ip3r (WT:  $1.0000 \pm 0.3180$ ,  $N=5$ ; Mut:  $1.9938 \pm 0.1457$ ;  $N=8$ ), total Ampk and pAmpk; densitometry shows pAmpk/total Ampk (WT:  $1.0000 \pm 0.2013$ ,  $N=5$ ; Mut:  $0.6950 \pm 0.0396$ ,  $N=8$ ). (D) CaMKII and pCaMKII; densitometry shows the pCaMKII/total CaMKII ratio (WT:  $1.0000 \pm 0.1566$ ,  $N=4$ ; Mut:  $0.6936 \pm 0.0309$ ,  $N=4$ ). (E) SERCA2 (WT:  $1.0000 \pm 0.2026$ ,  $N=3$ ; Mut:  $1.5468 \pm 0.0861$ ,  $N=3$ ). Data expressed as mean  $\pm$  SEM;  $p$  by unpaired Student's  $t$ -test.



chamber dilatation and electrical remodeling were already present at 3 months in the latter.<sup>18,19</sup> The age at which myocyte studies were carried out is roughly similar in the two studies (2–3 months), that is in a markedly different relationship with the development of a failing phenotype. As depression of SR function is a landmark of the remodeled myocardium<sup>20</sup> this might explain the different  $\text{Ca}^{2+}$  handling phenotypes observed in the two models.

SERCA2a functional downregulation is a common consequence of maladaptive remodeling and plays an undisputable role in evolution of contractile dysfunction and arrhythmogenesis in heart failure. By analogy, enhanced SERCA2a inhibition would easily explain the PLN R14del<sup>+/-</sup> ACM phenotype, as previously claimed.<sup>3</sup> The present results suggest instead that PLN

R14del<sup>+/-</sup> loses the ability to inhibit SERCA2a; the resulting “hyperdynamic”  $\text{Ca}^{2+}$  handling might look less plausible as a cause of reduced contractility. PLN knock-out, and the resulting “hyperdynamic state” of  $\text{Ca}^{2+}$  handling, may be well tolerated in TG mice;<sup>21</sup> nonetheless, it may lead to overt cardiomyopathy over longer time spans in hiPS-CMs.<sup>22</sup> In the latter case, cellular derangements were supported by  $I_{\text{NaL}}$  enhancement,<sup>22</sup> but it was unclear whether this represented a primary mutation effect. The present results show that ROS and CaMKII signaling (well-known  $I_{\text{NaL}}$  enhancers) was unperturbed at the pre-symptomatic stage of the mutation, thus suggesting that hyperdynamic  $\text{Ca}^{2+}$  handling per se may be inadequate to enhance  $I_{\text{NaL}}$ . The view that PLN loss of function may be harmful on the long run is also

supported by its association with ACM in human mutations,<sup>23</sup> by the observation that PLN-sarcolipin double knock-out triggers hypertrophic remodeling<sup>24</sup> and by the significant derangements occurring 2 months after PLN knock-out in hiPS-CMs.<sup>22</sup> Altogether, these findings indicate that constitutively unrestrained SERCA2a function may, in the long term, have a negative impact on myocyte biology. Notably, clinical ACM is indeed of late onset in PLN R14del<sup>+/-</sup> carriers.<sup>1</sup>

The discussion thus far assumes that PLN R14del detrimental effects depend on the impact of SERCA2a dysregulation on intracellular Ca<sup>2+</sup> dynamics; however, this is not necessarily the case. For instance, in the case of the PLN R9C mutation, late ACM developed independently of the sign of changes in SERCA2a function.<sup>25</sup> Thus, mechanisms linked to the PLN mutation, but perhaps independent of Ca<sup>2+</sup> dynamics, may derange myocyte biology. Unfortunately, this considerably broadens the array of mechanisms to be considered and, eventually, to be targeted with therapy (other than mutation reversal). Hence, we undertook a preliminary analysis of additional cell dysfunctions, potentially involved in the ACM of the PLN R14del<sup>+/-</sup> TG mouse. Although admittedly far from exhaustive, this analysis may provide relevant clues.

### 3.2 | Energy metabolism

Recent work on contracting hiPS-CMs organoids (EHTs) from a PLN R14del<sup>+/-</sup> carrier<sup>12</sup> detected abnormalities of the ER/mitochondrial compartment, reduced mitochondria number and function. Contraction force was halved in this preparation, despite a nearly normal SR function. Hence, we tested whether PLN R14del<sup>+/-</sup> TG affects energy metabolism in the mouse model, notably prior to the development of contractile dysfunction (i.e., as a primary abnormality). At least when quiescent (as dictated by the experimental setup), PLN R14del<sup>+/-</sup> CMs showed a substantial downregulation of energy metabolism, including its oxidative and anaerobic components (Figures 4 and 6).

Compatibility of overall depression of energy metabolism with grossly normal cardiac function in-vivo<sup>13</sup> is more surprising. Either function is maintained despite energy starvation, or ATP demand is reduced (at least at rest) in PLN R14del<sup>+/-</sup> CMs. To discriminate between these possibilities, we measured the  $I_{KATP}$  conductance (Figure 7), a surrogate of the ADP/ATP ratio, and activation of AMPK a major “energy starvation” signal (Figure 8). Albeit some heterogeneity was observed in  $I_{KATP}$  density, neither of the two measurements points to a mismatch between ATP production and demand under resting conditions. Why should PLN R14del<sup>+/-</sup> CMs consume significantly less ATP than WT ones? Under quiescence the Na<sup>+</sup>/K<sup>+</sup> pump

dominates as energy consumer.<sup>26</sup> Sarcolemmal Ca<sup>2+</sup> extrusion, by the energetically coupled NCX-Na<sup>+</sup>/K<sup>+</sup> pump complex, costs twice as much ATP as Ca<sup>2+</sup> recycling to the SR by SERCA2.<sup>27</sup> Therefore, lowering of SERCA2a  $K_{dCa}$ , as in PLN R14del<sup>+/-</sup> CMs, might theoretically alleviate the load on the Na<sup>+</sup>/K<sup>+</sup> pump and be energy saving. The reduction in NCX “conductance” (Figure S2), possibly an adaptation to SERCA2a dominance, would contribute to limit energy consumption. Coexistence of the energetic defect with normal ROS levels and mitochondrial membrane polarization (Figure S7) suggests that, at this stage, the former may reflect mitochondrial dysregulation, as opposed to overt damage. Increased OCR dependency on intracellular Ca<sup>2+</sup> (Figure 5) might underlie such dysregulation (see below). On the other hand, pacing unveiled energetic incompetence in Mut CMs. This suggests that hyperdynamic Ca<sup>2+</sup> handling may be inadequate to compensate for the metabolic defect when contraction dominates ATP consumption, thus perturbing the subtle balance preserving energy charge at rest.

### 3.3 | Coupling between Ca<sup>2+</sup> dynamics and energy metabolism

Mitochondrial Ca<sup>2+</sup> plays a pivotal role in the regulation of mitochondrial respiration and ATP synthesis. To test the involvement of altered Ca<sup>2+</sup> dynamics in the reduction of (resting) OCR, the latter was measured in the presence of cytosolic Ca<sup>2+</sup> chelation (BAPTA), or “functional deletion” of the SR store (THAPSI). Both interventions decreased OCR (Figure 5), thus confirming the role of Ca<sup>2+</sup>, and the SR contribution, in its regulation. Interestingly, maximal-, but not basal-OCR, was differentially regulated in Mut versus WT CMs. This can be tentatively interpreted by considering that, whereas basal OCR responds to multiple Ca<sup>2+</sup>-sensitive factors (including extra-mitochondrial ones), maximal OCR should depend exclusively on the intrinsic electron transport (ET) rate. ET rate is expectedly sensitive to matrix Ca<sup>2+</sup>, required to support the production of reduced substrates fuelling the ET reactions. This considered, the stronger sensitivity of maximal-OCR to BAPTA and THAPSI peculiar of Mut CMs may reflect increased Ca<sup>2+</sup> requirements of the reactions fuelling ET, or of ET reactions themselves. While this might be seen as adaptive to hyperdynamic Ca<sup>2+</sup> handling, energetic incompetence of Mut CMs after pacing indicates a genuine defect in energy production.

The link between Ca<sup>2+</sup> handling and energy metabolism abnormalities is still elusive. The metabolic response to PLN knock-out in hiPS-CMs is a transient increase in OCR, followed by mitochondrial damage only at a later stage.<sup>22</sup> This argues against hyperdynamic Ca<sup>2+</sup> handling

as a primary cause of mitochondrial dysfunction. Notably, while both PLN R14del<sup>+/-</sup> and PLN knock out induce a hyperdynamic state, in the latter PLN protein is missing. This may point to an additional pathogenetic mechanism in ACM caused by PLN R14del<sup>+/-</sup> but perhaps independent from changes in SERCA2a function.

### 3.4 | Transcript and protein analysis

Cell damage might be caused, independent of SERCA2a dysregulation, by direct toxicity of the mutant protein (ER-stress) and the resulting activation of the “unfolded protein response” (UPR).<sup>28</sup> ER-stress activation and reduced mitochondria abundance were indeed the main derangement detected in PLN R14del<sup>+/-</sup>.<sup>12</sup> In the present study, transcript and protein analysis (Figure 8; Figure S8) mainly yielded negative results, which may nonetheless be informative. Failure to detect activation of energy starvation signaling under rest is in line with unchanged cell energy charge (normal resting  $I_{KATP}$  density, Figure 7). Lack of activation of ROS scavenging genes, along with normal ROS content and mitochondrial membrane potential, stand for the absence of major mitochondrial damage under quiescence. Similarly, lack of CaMKII activation argues against early involvement of Ca<sup>2+</sup> decompartmentalization in disease pathogenesis.

## 4 | LIMITATIONS

Because of technical constraints, energy production and signaling were assessed in quiescent CMs. SERCA2a might be marginally activated in such condition and the presence of just a trend of OCR decrease in response to THAPSI (Figure 5D) supports this view. The cell metabolic state would be obviously different in contracting myocytes. This demands attention in referring each finding to the state (resting or contracting) under which measurements were carried out (clearly specified throughout the manuscript) and some speculation is necessarily involved in translating the study outcome to the contracting heart.

With the aim of disclosing initiating mechanisms, the present study evaluates mutation's effects before the development of overt cardiac abnormalities. As commonly occurs in cardiac remodeling, additional mechanisms may contribute to myocardial dysfunction at later stages.

The choice of sex uniformity to minimize variability fails to consider potential sex differences in determining the extent of mutation manifestations.

Due to limited availability of material, SERCA ATPase activity (Figure 1) was measured from 2 hearts per experimental group. However, multiple technical replicates were

obtained from each heart; furthermore, the result of this measurement is only part of the evidence leading to the conclusion that the mutation enhances SERCA2a function.

## 5 | MATERIALS AND METHODS

The methods are described here to the extent of allowing interpretation of results. A detailed description is given in the Data S1.

### 5.1 | Experimental model

The studies were performed on tissues from PLN R14del<sup>+/-</sup> (Mut) mice aged 8 to 12 weeks and their WT littermates (controls). In this age range, the animals are healthy; overt physical or echocardiographic signs of chamber remodeling or contractile dysfunction arise in this model at 18 months of age.<sup>13</sup> This is crucial to the interpretation of the observed changes as directly resulting from the mutation, rather than secondary to unspecific myocardial remodeling.

Myocytes were enzymatically dissociated with a manual perfusion method<sup>29</sup> which does not discriminate between right and left ventricles and studied within 24 h.

All experiments involving animals confirmed to the guidelines for Animal Care endorsed by the Milano-Bicocca and to the Directive 2010/63/EU of the European Parliament on the protection of animals used for scientific purposes.

### 5.2 | Measurements and techniques

- CPA-sensitive (SERCA2a) ATPase activity was measured in myocardial homogenates at multiple Ca<sup>2+</sup> concentrations; data points were fitted to a sigmoidal (Hill) function, from which the maximum velocity ( $V_{max}$ ) and Ca<sup>2+</sup> affinity [ $Kd_{Ca}$ ] parameters were estimated.
- Electrophysiological experiments were carried out by whole-cell patch clamp on isolated ventricular cardiomyocytes (CMs) in the ruptured- or perforated-patch configuration, as specified in the relevant Section 2.
- Cytosolic Ca<sup>2+</sup> was optically measured from isolated CMs by using Fluo 4-AM as the Ca<sup>2+</sup>-sensitive probe; fluorescence (F) was normalized to the value measured after prolonged quiescence (F<sub>0</sub>). Ca<sup>2+</sup> measurements were carried out in field-stimulated CMs, or V-clamped CMs, as specified in the relevant Section 2.
- OCR and PER were measured under basal and metabolically stressed conditions in quiescent CMs seeded

in multiwell plates using the Seahorse technology (Agilent Extracellular Flux Analyzer XFe96) in order to determine mitochondrial respiratory and glycolytic bioenergetics. All measurements were normalized to the (automatically counted) number of viable CMs in the measuring well. All the experimental conditions were represented in each plate to allow comparisons within the same experiment; the position of each condition in the plate was swapped between experiments to prevent technical bias. The preparations were exposed to reagents to obtain specific OCR and PER parameters, as described in the Section 5.3.

- ROS content of CMs was measured after incubation with the fluorescent probe DCFDA. Automated (unbiased) confocal *single-cell* fluorescence measurement was performed by Operetta CLS™ (Operetta– Perkin Elmer) at 40× magnification.
- Mitochondrial membrane potential ( $\Psi_m$ ) was measured from CMs using TMRE as probe. Stained CMs were seeded at the concentration  $2.5 \times 10^3$  per well. TMRE fluorescence was analyzed by confocal imaging at 63× magnification (Operetta CLS™). At the concentration used in the present study, TMRE works in “quenching mode,” that is emission increases as  $\Psi_m$  depolarizes.<sup>30</sup> At any rate, TMRE fluorescence signal was calibrated in each measurement by short-circuiting mitochondrial electron transport with FCCP.
- qRT-PCR was performed on mRNA extracted from myocardial samples and quantified by a NanoDrop spectrophotometer. qRT-PCR was performed with the primers reported in Table S1. All reactions were performed in a 384-well format. The relative quantities of specific mRNAs were obtained by the delta–delta Ct method with normalization to the housekeeping transcript glyceraldehyde 3-phosphate dehydrogenase (GAPDH).
- Western Blot Analysis was performed on RV samples. Total protein extracts were subjected to SDS-PAGE and transferred onto a nitrocellulose membrane, blocked for 1 h at room temperature and incubated overnight at 4°C with the appropriate primary antibodies (reported in Table S2). Peroxidase-conjugated secondary antibodies were then applied for 1 h and the peroxidase signal visualized using a chemiluminescent substrate. Blot images were acquired and blot densitometric analysis was performed by ImageJ software. Protein signals were normalized to that of the housekeeping proteins GAPDH or Tubulin.

### 5.3 | Experimental protocols

Significant parameters were extracted from the above measurements by applying suitable experimental protocols.

- $\text{Ca}^{2+}$  transients (CaT) were evaluated in intact CMs., field-stimulated at 1 Hz.  $\text{Ca}^{2+}$  transient amplitude (CaT amplitude),  $\text{Ca}^{2+}$  transient decay kinetics ( $\tau_{\text{decay}}$ ),  $\text{Ca}^{2+}$  transient rise-time ( $t_{\text{peak}}$ ) and diastolic  $\text{Ca}^{2+}$  (CaD) were measured. Rate-dependency of CaT properties was tested by stepwise increments in pacing rate (to 1, 1.3, 1.7, and 2 Hz).
- SR  $\text{Ca}^{2+}$  content was estimated in V-clamped CMs as the integral of the  $I_m$  (mostly representing  $I_{\text{NCX}}$ ) elicited by a caffeine (10 mM) pulse, applied after a loading train of V steps (–40 to 0 mV at 1 Hz).<sup>31</sup> To avoid extracellular  $\text{Ca}^{2+}$  influx, caffeine was dissolved in  $\text{Ca}^{2+}$ -free solution (containing 1 mM EGTA CsOH).
- The “gain” of  $\text{Ca}^{2+}$ -induced  $\text{Ca}^{2+}$  release (CICR) was measured in V-clamped CMs as the  $\text{Ca}^{2+}$  release/influx ratio, as previously described.<sup>32</sup>
- The fraction of SR  $\text{Ca}^{2+}$  content released by membrane excitation (fractional release) was calculated as the ratio between the amplitudes of V- and caffeine-triggered CaT.
- Information on NCX function was obtained by linear fitting of the trailing branch of the  $I_{\text{NCX}}/[\text{Ca}^{2+}]$  loops, recorded during caffeine-induced transients. The slope coefficient and the 0  $I_{\text{NCX}}$  intercept were used as surrogate of NCX “conductance” and cytosolic  $[\text{Ca}^{2+}]$  at electrochemical equilibrium, respectively.
- The  $\text{Ca}^{2+}$  uptake function of the SR was evaluated through a “SR reloading” protocol, applied under V-clamp; CaT and  $I_{\text{CaL}}$  were simultaneously recorded.<sup>33</sup> The SR was initially emptied by a caffeine pulse and progressively reloaded by a train (0.25 Hz) of 200 ms V steps from –40 to 0 mV. The following parameters were analyzed from each step of the protocol: (i) CaT amplitude, (ii) CICR gain, (iii)  $\tau_{\text{decay}}$ , (iv) CaD. The rate of increment of the former two parameters during the loading protocol reports the rate of SR refilling. The time constant of CaT decay ( $\tau_{\text{decay}}$ ) reports the rate of cytosolic  $\text{Ca}^{2+}$  clearance (the faster  $\text{Ca}^{2+}$  removal, the smaller  $\tau_{\text{decay}}$ ) within each step, i.e., at varying SR filling levels. CaD course reports the rate of cytosolic  $\text{Ca}^{2+}$  accumulation.
- OCR and PER were monitored during sequential exposure of preparations to Oligomycin A (ATP synthase inhibitor), FCCP (in OCR only, short-circuits the electron transfer chain, ETC), Rotenone/Antimycin (block ETC complexes I and III) or 2-deoxy-D-glucose (2DG in PER only, inhibits glycolysis). Functional parameters were derived as follows:
  - OCR parameters: (i) mitochondrial basal respiration = OCR before Oligomycin – OCR after Rotenone/Antimycin; (ii) mitochondrial maximal respiration = OCR after FCCP – OCR after Rotenone/Antimycin; (iii) spare respiratory

capacity = mitochondrial maximal respiration – mitochondrial basal respiration; (iv) non-mitochondrial respiration = OCR after Rotenone/Antimycin.

- PER parameters: (i) basal glycolysis = PER before Oligomycin – PER after 2DG; (ii) compensatory glycolysis = PER after Rotenone/Antimycin – PER after 2DG; (iii) glycolytic reserve = compensatory glycolysis – basal glycolysis; (iv) non-glycolytic acidification = PER after 2DG.
- $I_{KATP}$  was used as surrogate reporter of the ADP/ATP ratio (see validation in Figure S6B).  $I_{KATP}$  was measured as glibenclamide-sensitive current while holding membrane potential at  $-120$  mV (i.e., negative to  $K^+$  equilibrium potential) in the perforated-patch configuration. Measurements were performed in unstimulated myocytes (quiescence) and immediately after a train of pacing of pulses at 2 Hz.

## 5.4 | Statistical analysis

Statistical analysis was carried out with GraphPad Prism 8. Normality of distribution was assessed using D'Agostino-Pearson's normality test. Comparison of sample means was carried out with parametric or non-parametric tests, according to the data type (continuous or categorical) and distribution normality. Parametric or non-parametric ANOVA (with the respective post-hoc corrections) were used for multiple comparisons of continuous or categorical data respectively. In the case of repeated measurements (e.g., rate-dependency and SR loading protocols) a mixed-effects ANOVA model containing "Treatment" (WT vs. Mut, PST-3093 vs. Control) and "Variable" (rate or step #) factors was used. Significance of "Treatment  $\times$  Variable interaction" (i.e., difference between Treatments in their response to the Variable) was first tested; in its absence, significance of difference between Treatments at all Variable values was tested. In figures, data are presented as mean  $\pm$  SEM. Whenever the threshold for statistical significance was achieved, the following symbols were used: \* $p < 0.05$ , †  $p < 0.01$ , ‡  $p < 0.001$ . Throughout the text, the actual  $p$ -value for the comparison was reported as an index of robustness. For each experiment, the number of preparations or cells ( $n$ ) and the number of animals from which they were obtained ( $N$ ) are indicated in the respective figure legend.

## 6 | CONCLUSIONS

The present results extend our previous observation in patient-derived hiPS-CMs<sup>11</sup> to indicate that PLN R14del<sup>+/-</sup> may upregulate SERCA2a activity, thus

inducing hyperdynamic  $Ca^{2+}$  handling, in native mature CMs of the TG mouse. The mutation also results in a substantial downregulation of energetic metabolism at rest, not associated with signs of overt mitochondrial damage, but leading to energetic incompetence during pacing. Downregulation of energy production in resting mutant CMs might be seen as the "physiological" response to reduced ATP demand, expected from switch to SERCA2a dominance in  $Ca^{2+}$  handling. Nonetheless, increased OCR dependency on  $Ca^{2+}$  and pacing-induced energetic incompetence point to genuine mitochondrial dysfunction in Mut CMs.

While hyperdynamic  $Ca^{2+}$  handling is unlikely the primary cause of the metabolic defect at this disease stage, previous work suggests that toxicity of the mutant protein may be involved. Indeed, pronounced ER stress has been reported in PLN R14del<sup>+/-</sup> hiPS-CMs<sup>12</sup> and, despite the early disease stage, the present findings include activation of some signals related to unfolded protein response (UPR). Once initiated, UPR could be responsible for a host of cellular abnormalities, including major mitochondrial remodeling and SR damage.<sup>28</sup> Since many of these processes are  $Ca^{2+}$ -dependent, the view that ACM pathogenesis might be independent of hyperdynamic  $Ca^{2+}$  handling may not conflict with the observation that strong  $Ca^{2+}$  buffering may prevent phenotype development.<sup>12</sup>

Last but not least, the cellular mutation phenotype of the TG mouse described in the present study is mostly consistent with that of patient-derived hiPS-CMs,<sup>11,12</sup> thus providing cross-validation of these experimental models.

## 7 | THERAPEUTIC IMPLICATIONS

The initial hypothesis of SERCA2a superinhibition by PLN R14del<sup>+/-</sup> pointed to the therapeutic potential of PLN-displacing SERCA2a activators, now available as drugs.<sup>10,33,34</sup> The loss of SERCA2a function detected in the zebrafish TG model of the mutation, was indeed reversed by one of these compounds (istaroxime).<sup>5</sup> However, consistent with a loss of SERCA2a inhibition by PLN R14del<sup>+/-</sup>, the prototypical selective SERCA2a activator PST-3093, was totally ineffective in patient-derived hiPS-CMs<sup>11</sup> and TG mouse CMs (present results). This, and the likely involvement of pathogenetic mechanisms beyond SERCA2a dysregulation, may suggest to invest on mutation reversal,<sup>35</sup> or at least on improvement of mutant protein processing (e.g. by "chaperone" molecules), or reducing the impact of pathogenic PLN protein<sup>13,36</sup> as the most logical mechanism-based therapeutic approaches. Speaking of more generic approaches, countering the enhancement of sustained  $Na^+$  current (a common response

to cell stress) has proven effective in preventing the consequences of chronic upregulation of Ca<sup>2+</sup> cycling in hiPS-CMs.<sup>22</sup>

### AUTHOR CONTRIBUTIONS

**Francesco Lodola:** Conceptualization; project administration; supervision; writing – original draft. **Claudia Maniezzi:** Data curation; formal analysis; investigation; writing – original draft. **Marem Eskandr:** Data curation; formal analysis; investigation. **Chiara Florindi:** Data curation; formal analysis; investigation. **Mara Ferrandi:** Investigation; methodology. **Paolo Barassi:** Investigation; methodology. **Elena Sacco:** Data curation; formal analysis; supervision. **Valentina Pasquale:** Formal analysis; investigation. **Angela S. Maione:** Data curation; investigation; formal analysis. **Giulio Pompilio:** Supervision; resources. **Vivian Oliveira Nunes Teixeira:** Methodology. **Rudolf A. de Boer:** Funding acquisition. **Herman H. W. Silljé:** Funding acquisition; methodology. **Antonio Zaza:** Writing – original draft; conceptualization; funding acquisition; resources; supervision; validation; writing – review and editing.

### ACKNOWLEDGMENTS

The authors are grateful to Prof. Giuseppe Bianchi (Windtree Therapeutics) for supplying PST3093 and to Beatrice Ferè, and Daniele Martone for optimizing the Langendorff-Free isolation methodology.

### FUNDING INFORMATION

This work was funded by grants from CVie Therapeutics Limited for the development of PLN antagonists (to AZ) and from the European Union-Italian Ministry of University and Research – grant PNRR – M4C2-I1.3 Project PE\_0000019 “HEAL ITALIA” (to BtBs Department). The Operetta and Seahorse platforms were acquired through the MUR-Competitive Grant for Excellent Departments (2018–2022) to University Milano-Bicocca. Generation of the PLN-R14del murine model was supported by grants from the Netherlands Heart Foundation (CVON PREDICT2, grant 2018-30; and CVON DOUBLE DOSE, grant 2020B005; CarMa 01-003-2022-0358), by a grant from the leDucq Foundation (Cure PhosphoLambaN induced Cardiomyopathy [Cure-PLaN]), by a grant from the European Research Council (ERC CoG 818715, SECRETE-HF) and grants from the Netherlands Heart Institute (NLHI) and the PLN heart Foundation.

### CONFLICT OF INTEREST STATEMENT

AZ recipient of research funding by CVie Therapeutics Limited (Taipei, Taiwan), WindTree Therapeutics (Warrington, USA) for research on PLN antagonists. The UMCG which employed/employs several of the authors

received research grants and/or fees from AstraZeneca, Abbott, Boehringer Ingelheim, Cardior Pharmaceuticals GmbH, Ionis Pharmaceuticals, Inc., Novo Nordisk, and Roche. Dr. de Boer has had speaker engagements with Abbott, AstraZeneca, Bayer, Bristol Myers Squibb, Novartis, and Roche. The views and opinions expressed in this manuscript are those of the authors only and do not necessarily reflect those of the European Union or the European Commission. Neither the European Union nor the European Commission can be held responsible for them.

### DATA AVAILABILITY STATEMENT

The authors confirm that the data supporting the findings of this study are available within the article and/or its supplementary materials. The data that support the findings of this study are available from the corresponding author upon request.

### ORCID

Elena Sacco  <https://orcid.org/0000-0002-3190-7671>

Francesco Lodola  <https://orcid.org/0000-0002-3506-5619>

### REFERENCES

- van der Zwaag PA, van Rijsingen IAW, Asimaki A, et al. Phospholamban R14del mutation in patients diagnosed with dilated cardiomyopathy or arrhythmogenic right ventricular cardiomyopathy: evidence supporting the concept of arrhythmogenic cardiomyopathy. *Eur J Heart Fail.* 2012;14(11):1199-1207.
- van der Zwaag PA, van Rijsingen IAW, de Ruiter R, et al. Recurrent and founder mutations in The Netherlands—Phospholamban p.Arg14del mutation causes arrhythmogenic cardiomyopathy. *Neth Heart J.* 2013;21(6):286-293.
- Haghighi K, Kolokathis F, Gramolini AO, et al. A mutation in the human phospholamban gene, deleting arginine 14, results in lethal, hereditary cardiomyopathy. *Proc Natl Acad Sci.* 2006;103(5):1388-1393.
- Stroik DR, Ceholski DK, Bidwell PA, et al. Viral expression of a SERCA2a-activating PLB mutant improves calcium cycling and synchronicity in dilated cardiomyopathic hiPSC-CMs. *J Mol Cell Cardiol.* 2020;138:59-65.
- Kamel SM, van Opbergen CJM, Koopman CD, et al. Istaroxime treatment ameliorates calcium dysregulation in a zebrafish model of phospholamban R14del cardiomyopathy. *Nat Commun.* 2021;12(1):7151.
- Vafiadaki E, Haghighi K, Arvanitis DA, Kranias EG, Sanoudou D. Aberrant PLN-R14del protein interactions intensify SERCA2a inhibition, driving impaired Ca<sup>2+</sup> handling and arrhythmogenesis. *Int J Mol Sci.* 2022;23(13):6947.
- Ceholski DK, Trieber CA, Young HS. Hydrophobic imbalance in the cytoplasmic domain of Phospholamban is a determinant for lethal dilated cardiomyopathy. *J Biol Chem.* 2012;287(20):16521-16529.
- Hughes E, Middleton DA. Comparison of the structure and function of Phospholamban and the Arginine-14 deficient



- mutant associated with dilated cardiomyopathy. *PLoS One*. 2014;9(9):e106746.
9. Vostrikov VV, Soller KJ, Ha KN, Gopinath T, Veglia G. Effects of naturally occurring arginine 14 deletion on phospholamban conformational dynamics and membrane interactions. *Biochim Biophys Acta*. 2015;1848(1):315-322.
  10. Arici M, Ferrandi M, Barassi P, et al. Istaroxime metabolite PST3093 selectively stimulates SERCA2a and reverses disease-induced changes in cardiac function. *J Pharmacol Exp Ther*. 2023;384(1):231-244.
  11. Badone B, Ronchi C, Lodola F, et al. Characterization of the PLN p.Arg14del mutation in human induced pluripotent stem cell-derived cardiomyocytes. *Int J Mol Sci*. 2021;22:13500.
  12. Cuello F, Knaust AE, Saleem U, et al. Impairment of the ER/mitochondria compartment in human cardiomyocytes with PLN p.Arg14del mutation. *EMBO mol Med*. 2021;13:e13074. doi:10.15252/emmm.202013074
  13. Eijgenraam TR, Boukens BJ, Boogerd CJ, et al. The phospholamban p.(Arg14del) pathogenic variant leads to cardiomyopathy with heart failure and is unresponsive to standard heart failure therapy. *Sci Rep*. 2020;10(1):9819.
  14. Lipskaia L, Chemaly ER, Hadri L, Lompre A-M, Hajjar RJ. Sarcoplasmic reticulum Ca<sup>2+</sup> ATPase as a therapeutic target for heart failure. *Expert Opin Biol Ther*. 2010;10(1):29-41.
  15. Mahaney JE, Albers RW, Waggoner JR, Kutchai HC, Froehlich JP. Intermolecular conformational coupling and free energy exchange enhance the catalytic efficiency of cardiac muscle SERCA2a following the relief of Phospholamban inhibition. *Biochemistry*. 2005;44(21):7713-7724.
  16. Kefaloyianni E, Bao L, Rindler MJ, et al. Measuring and evaluating the role of ATP-sensitive K<sup>+</sup> channels in cardiac muscle. *J Mol Cell Cardiol*. 2012;52(3):596-607.
  17. Cleary SR, Teng ACT, Phillips TA, et al. A dilated cardiomyopathy mutation of phospholamban, R14del, increases phospholamban pentamer stability. *Biophys J*. 2023;122(3):527a.
  18. Haghghi K, Gardner G, Vafiadaki E, et al. Impaired right ventricular calcium cycling is an early risk factor in R14del-Phospholamban arrhythmias. *J Pers Med*. 2021;11(6):502.
  19. Dave J, Raad N, Mittal N, et al. Gene editing reverses arrhythmia susceptibility in humanized PLN-R14del mice: modelling a European cardiomyopathy with global impact. *Cardiovasc Res*. 2022;118:3140-3150.
  20. Lehnart SE, Maier LS, Hasenfuss G. Abnormalities of calcium metabolism and myocardial contractility depression in the failing heart. *Heart Fail Rev*. 2009;14(4):213-224.
  21. Slack JP, Grupp IL, Dash R, et al. The enhanced contractility of the Phospholamban-deficient mouse heart persists with aging. *J Mol Cell Cardiol*. 2001;33(5):1031-1040.
  22. Jiang Y, Li X, Guo T, et al. Ranolazine rescues the heart failure phenotype of PLN-deficient human pluripotent stem cell-derived cardiomyocytes. *Stem Cell Reports*. 2022;17(4):804-819.
  23. Haghghi K, Kolokathis F, Pater L, et al. Human phospholamban null results in lethal dilated cardiomyopathy revealing a critical difference between mouse and human. *J Clin Invest*. 2003;111(6):869-876.
  24. Shanmugam M, Gao S, Hong C, et al. Ablation of phospholamban and sarcolipin results in cardiac hypertrophy and decreased cardiac contractility. *Cardiovasc Res*. 2011;89(2):353-361.
  25. Schmitt JP, Ahmad F, Lorenz K, et al. Alterations of Phospholamban function can exhibit cardiotoxic effects independent of excessive sarcoplasmic reticulum Ca<sup>2+</sup>-ATPase inhibition. *Circulation*. 2009;119(3):436-444.
  26. Readnower RD, Brainard RE, Hill BG, Jones SP. Standardized bioenergetic profiling of adult mouse cardiomyocytes. *Physiol Genomics*. 2012;44(24):1208-1213.
  27. Sakata S, Lebeche D, Sakata N, et al. Restoration of mechanical and energetic function in failing aortic-banded rat hearts by gene transfer of calcium cycling proteins. *J Mol Cell Cardiol*. 2007;42(4):852-861.
  28. Senft D, Ronai ZA. UPR, autophagy, and mitochondria cross-talk underlies the ER stress response. *Trends Biochem Sci*. 2015;40(3):141-148.
  29. Ackers-Johnson M, Li PY, Holmes AP, O'Brien SM, Pavlovic D, Foo RS. A simplified, Langendorff-free method for concomitant isolation of viable cardiac myocytes and nonmyocytes from the adult mouse heart. *Circ Res*. 2016;119(8):909-920.
  30. Perry SW, Norman JP, Barbieri J, Brown EB, Gelbard HA. Mitochondrial membrane potential probes and the proton gradient: a practical usage guide. *Biotechniques*. 2011;50(2):98-115.
  31. Varro A, Negretti N, Hester SB, Eisner DA. An estimate of the calcium content of the sarcoplasmic reticulum in rat ventricular myocytes. *Pflugers Arch*. 1993;423(1-2):158-160.
  32. Alemanni M, Rocchetti M, Re D, Zaza A. Role and mechanism of subcellular Ca<sup>2+</sup> distribution in the action of two inotropic agents with different toxicity. *J Mol Cell Cardiol*. 2011;50(5):910-918.
  33. Rocchetti M, Besana A, Mostacciolo G, et al. Modulation of sarcoplasmic reticulum function by Na<sup>+</sup>/K<sup>+</sup> pump inhibitors with different toxicity: digoxin and PST2744 [(E,Z)-3-((2-aminoethoxy)imino)androstane-6,17-dione hydrochloride]. *J Pharmacol Exp Ther*. 2005;313(1):207-215.
  34. Carubelli V, Zhang Y, Metra M, et al. Treatment with 24 hour istaroxime infusion in patients hospitalised for acute heart failure: a randomised, placebo-controlled trial. *Eur J Heart Fail*. 2020;22(9):1684-1693.
  35. Stillitano F, Turnbull IC, Karakikes I, et al. Genomic correction of familial cardiomyopathy in human engineered cardiac tissues. *Eur Heart J*. 2016;37(43):3282-3284.
  36. Stege NM, Eijgenraam TR, Oliveira Nunes Teixeira V, et al. DWORF extends life span in a PLN-R14del cardiomyopathy mouse model by reducing abnormal sarcoplasmic reticulum clusters. *Circ Res*. 2023;133:1006-1021.

## SUPPORTING INFORMATION

Additional supporting information can be found online in the Supporting Information section at the end of this article.

**How to cite this article:** Maniezzi C, Eskandr M, Florindi C, et al. Early consequences of the phospholamban mutation PLN-R14del<sup>+/-</sup> in a transgenic mouse model. *Acta Physiol*. 2024;00:e14082. doi:10.1111/apha.14082